

Vibration Assisted Polariton Wavefunction Evolution in Organic Nanofibers.

Vladimir Al. Osipov^{1,*} and Boris Fainberg^{2,1,†}

¹*H.I.T.-Holon Institute of Technology, 52 Golomb Street, Tel Aviv 69978, Israel*

²*School of Chemistry, Tel Aviv University, POB 305 Holon 5810201, Israel*

(Dated: July 19, 2022)

Formation of the composite photonic-excitonic particles, known as polaritons, is an emerging phenomenon in materials possessing strong coupling to light. The organic-based materials besides the strong light-matter interaction also demonstrate strong interaction of electronic and vibrational degrees of freedom. We utilize the Dirac-Frenkel variation principle to derive semiclassical equations for the vibration-assisted polariton wavefunction evolution when both types of interactions are treated as equally strong. By means of the approach, we study details of the polariton relaxation process and the mechanism of the polariton light emission. In particular, we propose the photon emission mechanism, which is realized when the polariton wave package exceeds the geometrical size of the nanosystem. To verify our conclusions we reproduce the fluorescence peak observed in experiment (Takazawa *et.al.* Phys.Rev.Let. **105**:07401, 2010) and estimate the light-matter interaction parameter.

PACS numbers:

When dye molecules are embedded in microstructures such as microcavities and nanofibers, the strong light-matter interaction can lead to formation of composite photon-exciton particles, known as exciton polaritons (EP), see¹⁻³ and references therein. The systems with strong coupling draw a lot of attention due to their potential to cause changes in chemical reaction rates⁴, to form high-temperature EP Bose-Einstein condensate^{3,5,6}, and to show long-range particle propagation⁷⁻¹⁰. The concept, generally used to describe the polaritons in the organic-based devices, deal with the Frenkel excitons, possessing the large binding energy and the large oscillator strength, and the light modes entangled to them. Due to anticrossing of the light and the exciton dispersions, the light-matter interaction splits the EP dispersion curve onto lower and upper branches. The splitting is governed by the strength of the light-matter interaction parameter g . In organic materials g can reach significant values, up to^{2,10} 1eV. The strong interaction of electronic and vibrational degrees of freedom, an inherent property of organic materials, essentially increases the EP stability and admits dynamic rearrangements in polariton systems: from boson-like condensation of polaritons³ to their relaxation¹¹, and transport¹⁰. In the spectra of organic-based polariton devices the interaction with vibrations is revealed through the vibronic replicas of the polariton dispersion curves¹²⁻¹⁴. Therefore, both the interaction between light and molecular electron density, and the interaction of electron density with the molecular backbone vibrations must be considered as equally strong¹⁵⁻¹⁷.

In Refs.^{14,18,19} the vibronic progression in EP fluorescent spectra has been explained with the help of the semiclassical rate equations, which describe the polariton states population evolution. However, for solution of transport and other dynamical problems, knowledge of the wavefunction evolution and spatial propagation

might be more important. A few attempts to describe the polariton wavefunction has been done in Refs.^{20,21} without accounting of vibrations. In present article we derive from ab initio Hamiltonian a set of equations for the vibration assisted polariton wavefunction evolution.

In our set up the unpolarized laser light excites polaritons in a perfect molecular crystal. The free photons dispersion is $\omega_q = cq/\sqrt{\epsilon_0}$, where $c/\sqrt{\epsilon_0}$ is the speed of light in the media, and q is the wavevector absolute value. The polaritonic part, \hat{H}_{pol} , of the total Hamiltonian, $\hat{\mathcal{H}} = \hat{H}_{pol} + \hat{H}_{vib} + \hat{H}_{ex}$ is modelled by the standard quadratic form Hamiltonian²²,

$$\hat{H}_{pol} = \hbar \sum_q \Lambda_{+q} Q_q^\dagger Q_q + \Lambda_{-q} P_q^\dagger P_q, \quad (1)$$

in terms of the upper and lower polariton operators,

$$Q_q = \cos \phi_q A_q + i \sin \phi_q B_q; \quad (2)$$

$$P_q = -\sin \phi_q A_q + i \cos \phi_q B_q. \quad (3)$$

The upper and lower branches of the dispersion curve are $\Lambda_{\pm q} = \frac{1}{2} \left(\omega_q + \omega_{ex} \pm \sqrt{(\omega_q - \omega_{ex})^2 + 4g^2} \right)$, where g is the light-matter interaction strength parameter and ω_{ex} is the exciton energy. The bosonic operators A_q (eqs. 2, 3) are the photon annihilation operators. The exciton operators $B_q = \frac{1}{\sqrt{N}} \sum_m e^{-iqm} b_m$ (N – the number of molecules, b_m is the annihilation operator of an excitation on the m th molecule) under the standard assumption of small number of excitations also satisfy the standard bosonic commutator relations, so do the polariton operators Q_q and P_q . The “Hopfeld angle” (see insert in fig. 2 a) is defined as $\cos 2\phi_q = \frac{\omega_q - \omega_{ex}}{\Lambda_{+q} - \Lambda_{-q}}$ and ranges from 0 to $\pi/2$. At the anticrossing point $\omega_q = \omega_{ex}$ (AP) $\phi_q = \pi/4$.

The polariton Hamiltonian \hat{H}_{pol} is diagonalizable in the orthonormal basis $|q, (u, M)\rangle$. Each $|q, (u, M)\rangle$ con-

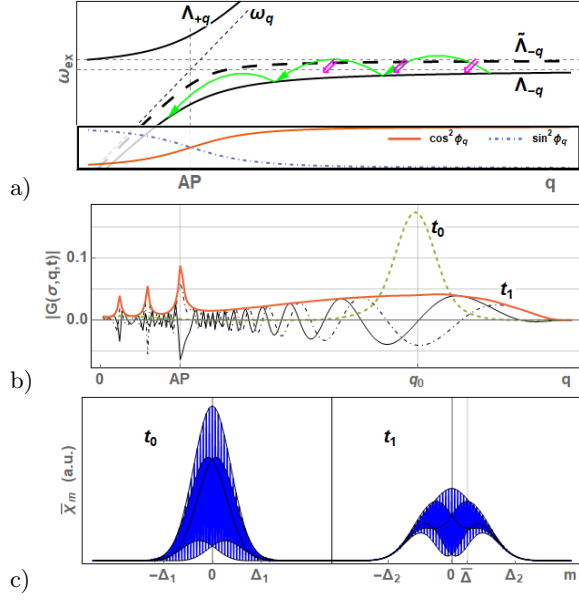


FIG. 1: (a) The EP dispersion curves $\Lambda_{\pm q}$ and dispersion curve of the exciton reservoir ($\tilde{\Lambda}_{-q}$). The evolution of the polariton wavefunction starts from the decay of the reservoir exciton states (the red arrows \Rightarrow) and slither across the dispersion curve Λ_{-q} (green thin arrows). AP denotes the anti-crossing point. In the insert: the Hopfield coefficients v.s. the momentum q ; (b) The typical distribution (thick solid) of the coefficient $|\mathcal{G}(\sigma, q, t)|$ plotted v.s. q obtained from numerical solution of eqs. (7, 8) subject to the initial normalized Gaussian distribution (thick dashed) localised at q_0 . The real and imaginary parts of $\mathcal{G}(\sigma, q, t)$ are shown by thin curves; (c) The factor $\bar{X}_m(t)$ (eq. 9) is plotted v.s. m for two instants of time ($t_1 > t_0 \sim 0$).

sists of M polariton particles excited with the momentum q : among them $M - u$ are the low-energy (Λ_{-q}) particles, which are entangled with the u high-energy (Λ_{+q}) particles. The non-zero matrix elements of the polariton Hamiltonian are³⁶ $\langle q, (u, M) | \hat{H}_{pol} | q, (u, M) \rangle = M\Lambda_{-q} + u(\Lambda_{+q} - \Lambda_{-q})$. Contrary to the condensation problem, the transport problem allows to restrict the consideration by the case of a single polariton particle. In what follows we assume that $M = 1$ and do not write the index M any more.

The vibrational part, \hat{H}_{vib} , is modelled by a number of harmonic oscillators ($\mu = 0, 1, \dots$) coupled to each molecule m ,

$$\begin{aligned} \hat{H}_{vib} = & \hbar \sum_{m,\mu} \Omega_\mu X_\mu (c_{m,\mu}^\dagger + c_{m,\mu}) b_m^\dagger b_m \\ & + \hbar \sum_{m,\mu} \Omega_\mu c_{m,\mu}^\dagger c_{m,\mu} + \hat{H}_{bath} (c_{m,\mu}^\dagger, c_{m,\mu}), \end{aligned} \quad (4)$$

The optically active vibration modes (operators $c_{m,\mu}$ and $c_{m,\mu}^\dagger$) interact with the dark vibration modes through the thermal bath Hamiltonian \hat{H}_{bath} . The frequencies Ω_μ and the oscillator equilibrium coordinates shifts X_μ in

the excited electronic state, are assumed to be equal for each m .

The exciton Hamiltonian \hat{H}_{ex} accounts for the inter-molecular interactions and imparts the momentum dependence to the exciton dispersion²³ ω_{ex} . In case of weakly coupled H-aggregated molecules (below we consider only this case) the short-range Frenkel exciton effective mass is large and we can neglect the q -dependence in ω_{ex} . Note that the accounting of the vibrations shifts the energy of the molecular optical transition by half of the Stokes' shift: $\omega_{ex} \rightarrow \omega_{ex} + \sum_\mu \Omega_\mu X_\mu^2$.

In organic molecules the frequency of the highest-frequency optically active (HFOA) mode is of one order of magnitude smaller ($\Omega_0 \sim 1000 - 1500 \text{ cm}^{-1}$) than the excitation energy ω_{0-0} (fig. 2 b) and $X_0 \sim 0.7$. The HFOA modes are responsible for the vibronic repetitions in spectra. The low-frequency optically active (LFOA) modes' frequencies (Ω_μ with $\mu = 1, \dots$) are comparable with the thermal energy $kT \sim 30 \text{ meV}$, and the molecule equilibrates over the LFOA modes almost immediately (several picoseconds) after the excitation. One can effectively separate the polaritons corresponding to the [0]-[1] and to the [0]-[0] transitions. For the [0]-[1] case the interaction parameter g is suppressed by the Franck-Condon factor $X_0 e^{-X_0^2/2}$. The dispersion curve with the effective coupling $gX_0 e^{-X_0^2/2}$ goes closer to the AP (see the curve $\tilde{\Lambda}_{-q}$ in fig. 1 a). This makes the polariton formation channel less efficient than the channel of rapid non-radiative decay to the state [0].

The basis of coherent states, $|\sigma\rangle \equiv \prod_{m,\mu} |\sigma_{m,\mu}\rangle$, provides a convenient description for LFOA vibrations. Each coherent state is parametrized by multidimensional complex-valued vector $\sigma_{m,\mu}$, which encodes the coherent state center (classical momentum and coordinate)³⁷. To describe evolution of the expansion coefficients $\mathcal{F}(\sigma, q, t)$ and $\mathcal{G}(\sigma, q, t)$ we generalize the polariton basis set by introducing the time-dependent basis set $|\sigma(t), q, u\rangle$. Then we make use the approach, which is based on the Dirac-Frenkel variation principle and useful for description of quantum dynamics in systems with large number of vibration modes²⁴⁻²⁷. In the extended basis the EP wavefunction has the expansion $|\Psi(t)\rangle = \sum_q \mathcal{F}(\sigma, q, t) e^{i\Lambda_{+q}t} |\sigma, q, 1\rangle + \mathcal{G}(\sigma, q, t) e^{i\Lambda_{-q}t} |\sigma, q, 0\rangle$. Variation of the Schrödinger equation $\langle \Psi | i\hbar \frac{d}{dt} - \hat{H} | \Psi \rangle = 0$ with respect to the bra-vector and equating to zero each term coming from the independent variations δF , δG , and $\delta \sigma_{m,\mu}$ yields the system of equations of motion. For $u = 0$ it is

$$\delta \sigma_{m,\mu}: \quad \mathcal{G}^*(\sigma, q, t) \langle \sigma, q, 0 | c_{m,\mu} \left(i\hbar \frac{d}{dt} - \hat{H} \right) | \Psi \rangle = 0; \quad (5)$$

$$\delta \mathcal{G}: \quad \langle \sigma, q, 0 | i\hbar \frac{d}{dt} - \hat{H} | \Psi \rangle = 0. \quad (6)$$

The eqs. (5), (6) completely describe evolution of the polariton wavefunction, subject to the initial conditions. Below we consider their explicit form in the mean field semiclassical approximation and neglect the upper

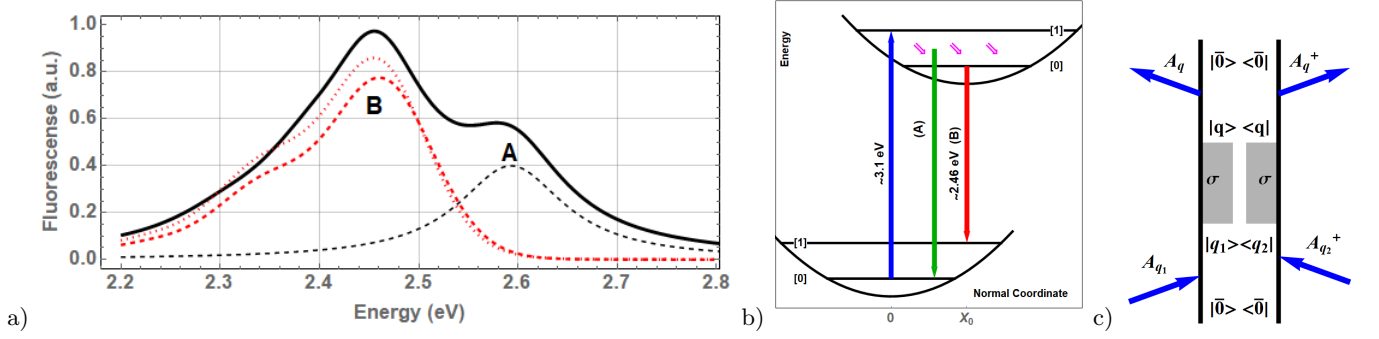


FIG. 2: (a) The PL spectrum (solid black) of the thiocyanine-dye nanofiber compared with the PL monomer (red dashed) and H-aggregate (red dotted) spectra, reconstructed from^{10,32–34}. The Lorentzian peak A is positioned at 2.593eV and the peak B maximum is at 2.457eV; (b) Jablonski diagram of HFOA transitions in the molecular aggregate; (c) The ladder-like diagram depicting the maximal contribution to the EP PL spectrum: two polaritons (vertical lines), initially created as the conjugated photons with the momentum q_1 and q_2 , evolve due to interaction with the vibrational bath (σ) to AP and decay from there into two coherent photons (A_q, A_q^\dagger), which are detected by detector.

branch of polariton states and quantum transitions from one branch to the other, i.e. $\mathcal{F}(\sigma, q, t) \equiv 0$ and equations for $u = 1$ become trivial. Explicit form of the equations of

motion for the quantum amplitude $\mathcal{G}(\sigma, q, t)$ and $\sigma_{m,\mu}(t)$ is

$$\frac{d\mathcal{G}(\sigma, q, t)}{dt} = -i \sum_{\Delta q} \mathcal{G}(\sigma, q - \Delta q, t) \sum_{m,\mu} \Omega_\mu X_\mu (\sigma_{m,\mu}^* + \sigma'_{m,\mu}) \left[\frac{e^{-i\Delta q m}}{N} e^{-i(\Lambda - (q - \Delta q) - \Lambda - q)t} \cos \phi_q \cos \phi_{q - \Delta q} - \delta_{\Delta q, 0} \frac{\bar{\chi}_m(t)}{2} \right] \quad (7)$$

$$\frac{d\sigma_{m,\mu}}{dt} = -i\Omega_\mu \left(\sigma_{m,\mu} + X_\mu \bar{\chi}_m(t) + \frac{1}{\hbar\Omega_\mu} \frac{\partial}{\partial \sigma_{m,\mu}^*} H_{Bath}(\sigma^*, \sigma) \right), \quad \mu = 1, 2 \dots \quad (8)$$

$$\bar{\chi}_m(t) = \frac{1}{N} \sum_{q,q'} \mathcal{G}^*(\sigma, q, t) \cos \phi_q e^{-i(\Lambda - q' - \Lambda - q)t - i(q - q')m} \cos \phi_{q'} \mathcal{G}(\sigma, q', t). \quad (9)$$

Eq. (8) follows from eq. (5) when the scalar product $\langle \sigma | \sigma' \rangle$ is replaced by $\delta(\sigma - \sigma')$. This semi-classical approximation is valid when the number of vibration modes is large. Eq. (8) is a classical Newton's equations of an oscillator interacting with a bath, which equilibrium coordinate is shifted from zero by $X_\mu \bar{\chi}_m(t)$. The factor $\bar{\chi}_m$ (eq. 9) is the quantum expectation value of the polariton state projection on the exciton subspace. At the derivation of eq. (8) to avoid instabilities (see discussion in Ref.²⁷) we make summation over all q and thus immerse the problem into the mean-field context. The first equation (eq. 7) describes redistribution of the polariton wavefunction in the momentum space, which happens due to the energy flux from the polariton subsystem to the optically active vibrations and eventually to the bath. The prime at $\sigma'_{m,\mu}$ in eq. (7) means that its value has to be taken at the previous instant of time. The emerging imaginary part in the term $\sigma_{m,\mu}^* + \sigma'_{m,\mu}$ is responsible for the overall decrease of the quantum probability $|G(\sigma, q, t)|^2$ due to redistribution over non-polaritonic degrees of freedom. Note, that the H_{Bath} Hamiltonian also includes the phonon-phonon interaction

terms. In what follows we use the reasonable for molecular crystals assumption of uncorrelated optical vibration modes, i.e. no dispersion in the optical branch and all $\sigma_{m,\mu}$ are independent, while the acoustic phonons form the thermal bath.

The overdamped Brownian oscillator model^{28–31} provides a general and convenient way for incorporating the nuclear motion into the numerical study of the problem. Under assumption of continuous distribution of the oscillators parameters Ω_μ and X_μ , the effective dimensionless oscillator coordinate $u_m \equiv \sqrt{2} < \sum_\mu \Omega_\mu X_\mu \text{Re} \{ \sigma_{m,\mu} \} >$, where the averaging is taken over the Gaussian stochastic random force acting from the side of the bath, satisfies the irreversible equation of motion $\dot{u}_m = \gamma^{-1} \left(\bar{\chi}_m(t) \sum_\mu \Omega_\mu X_\mu^2 - u_m \right)$. In case of large damping γ we use the approximation $\sum_\mu \Omega_\mu X_\mu (\sigma_{m,\mu}^* + \sigma'_{m,\mu}) \simeq 2\sqrt{2}u_m - i\dot{\bar{\chi}}_m(t)\sqrt{2}\gamma^{-1}\Delta t \sum_\mu \Omega_\mu X_\mu^2$. For convenience we assume that initially all vibrations are in the ground state, $u_m(0) = 0$, while $G(\sigma, q, t = 0)$ is distributed over various momenta far from AP (see Fig. 1 b).

The typical numerical solution for the coefficient

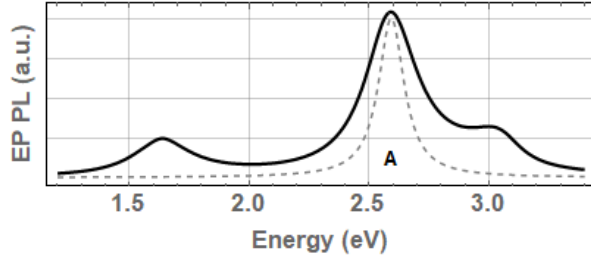


FIG. 3: The PL spectrum (solid line) calculated from the numerical equilibrium wavefunction (at $t_1 \sim 100fs$). The parameters $\omega_{ex} = 3.1eV$, $g = 0.69eV$, $\Gamma = 0.1eV$, the momentum cut-off $5.00 \times 10^8 m^{-1}$, $q_0 = 1.08 \times 10^8 m^{-1}$ and the AP momentum $q_{AP} = 2.13 \times 10^7 m^{-1}$. The dashed Lorentzian line A is the same as in Fig. 2 a.

$\mathcal{G}(\sigma, q, t)$ is given in fig. 1 b. The polariton wavefunction, during its evolution, scatters on the AP and forms very fast ($\sim 10fs$) an interference pattern with the highest peak at AP. It is worth mentioning, that the structure of the wavefunction is not an arbitrary but follows from the solution of eq. (7) in the steady state regime (see further publications for details). The factor $\bar{\chi}_m$ (eq. 9) is plotted in fig. 1 c. It is a composition of interfering wave packets. Their amplitudes decrease as the photon (small- q) part of the polariton wavefunction grows. The factor $\chi_m(t)$ can be represented as a sum of interfering packages of two types: diffusive and moving. The diffusive package localized at $m = 0$ arises from interference of the large- q smooth profiles of $\mathcal{G}(\sigma, q, t)$ and its slow spreading is controlled by the dispersion in the velocities, $\frac{d}{dq} \Lambda_{-q}$. The moving packages originate from the wavefunction sharp peaks located at AP and in the vicinity (fig. 1 b). At our choice of the model parameters (see caption in fig. 3) the speed of the AP peak package is of order 2.3 nm/fs (the position of its maximum at $t_1 = 100fs$ is $\bar{\Delta} \sim 230nm$, see fig. 1 c). Having set the typical Frenkel exciton size to $\sim 0.5nm$, one obtains $\bar{\Delta} \sim 460$ excitons and, for reference, $2\Delta_1 \sim 1.5\mu m \sim 3000$ excitons and $2\Delta_2 \sim 1.9\mu m \sim 4000$ excitons.

The experimental frequency-resolved PL spectrum (fig. 2 a) of the straight long thin ($200nm \times 600nm \times 18\mu m$) thiocyanine-dye H-aggregates nanofiber measured after excitation by unpolarized laser light with $\lambda = 405nm$ ($hc/\lambda \sim 3.06eV$) was reported in ref.³². The experimentally observed nanofiber PL spectrum in its central part (peak B in fig. 2 a) almost coincides with the H-aggregate and the monomer PL spectra^{10,33,34}, which are reproduced on the same plot for comparison. The A peak, however, finds no counterpart in the aggregate and/or monomer spectra and, thus, has to be explained by the polariton fluorescence. The diagram of transitions given in ref.¹⁰, in our opinion, misinterprets the fiber spectrum by addressing all its peaks solely to the decay of various excitonic states. Instead, we suggest the

level structure presented in fig. 2 b.

To compare our approach with experiment we estimate the position of the EP PL spectrum peak by means of the formula $PL(\omega) \propto \sum_q \frac{\hbar\omega|\mathcal{G}(\sigma, q, t_1)|^2 \sin^2 \phi_q}{(\omega - \Lambda_{-q})^2 + \Gamma^2}$, where the wavefunction coefficients are taken at some (large) time t_1 . The origin of the formula can be explained by the ladder-like diagram depicted in fig. 2 c (see text in the caption). We justify our approximate formula by the fact that the contributing peaks are sharp ($\Delta q \sim 7 \times 10^6 m^{-1}$) and start to form very early ($\sim 10fs$). The polaritons, initially created within a wide range of wavevectors, evolve quite long time ($t_1 \sim 100fs$) and decay by irradiation of two free photons with almost equal momenta q_{AP} . Note that the choice of the decay time t_1 is dictated by two circumstances: (i) it is the time of efficient equilibration and (ii) at this time the factor $\bar{\chi}_m$ maximum position reaches 200 nm, and thus goes out of the fiber width into the area where no more excitons can be created. The numerical spectrum is plotted in fig. 3 for the parameters given in the caption. Note that the ω_{ex} is chosen to be close to the absorption maxima of the H-aggregate¹⁰, while g is tuned to reproduce the experimental peak A. The obtained value of g is $\sim 0.7eV$.

Concluding remarks The quantum mechanical approach suggested in the article is derived from first principles and allows us to reproduce the position of the EP PL peak. We also demonstrate that the vibration assisted evolution of polaritons is a complex process taking place in both coordinate and momentum spaces. In particular, we propose a mechanism for the emission of polaritons due to the exit of the wave packet beyond the geometric limits of the nanosystem.

The approach being fully analytic opens a way for calculation of the polariton PL spectra by means of the nonlinear optical spectroscopy theoretical methods³¹ and the Greens' function theories. Note, that in its general formulation, the equations of motion allows to account the multiple-polaritons states, and the quantum transitions between the upper and lower dispersion branches (see further publications).

Acknowledgements. The work was supported by the Ministry of Science & Technology of Israel (grant No. 79518) and the grant RA1900000633 for cooperation between the Ariel University and the Holon Institute of Technology. The high-performance computational resources were provided by E.Kanzieper (through the ISF grant No. 428/18). Authors thank R.Riser for assistance in computations and H. Zoubi for useful discussions.

* Electronic address: Vladimir.AI.Osipov@gmail.com

† Electronic address: fainberg@hit.ac.il

[1] T.W. Ebbesen. Hybrid lightmatter states in a molecular and material science perspective. *Acc. Chem. Res.*,

- 49(11):2403–2412, 2016.
- [2] M. Hertzog, M. Wang, J. Mony, and K. Brjesson. Strong lightmatter interactions: a new direction within chemistry. *Chem. Soc. Rev.*, 48:937–961, 2019.
 - [3] A. Kavokin, J. J. Baumberg, G. Malpuech, and F. P. Laussy. *Microcavities*. Oxford University Press, Oxford, 2 edition, 2007.
 - [4] J.A. Hutchison, T. Schwartz, C. Genet, E. Devaux, and T.W.Ebbesen. Modifying chemical landscapes by coupling to vacuum fields. *Angewandte Chemie (International ed. in English)*, 51(7):15921596, February 2012.
 - [5] J. Kasprzak, M. Richard, S. Kundermann, and et al. Boseeinstein condensation of exciton polaritons. *Nature*, 443:409414, 2006.
 - [6] M S Skolnick, T A Fisher, and D M Whittaker. Strong coupling phenomena in quantum microcavity structures. *Semiconductor Science and Technology*, 13(7):645–669, jul 1998.
 - [7] S. Hou, M. Khatoniar, K. Ding, Y. Qu, A. Napolov, V. M. Menon, and S. R. Forrest. Ultralong-range energy transport in a disordered organic semiconductor at room temperature via coherent exciton-polariton propagation. *Advanced Materials*, 32(28):2002127, 2020.
 - [8] G.G. Rozenman, K. Akulov, A. Golombek, and T. Schwartz. Long-range transport of organic exciton-polaritons revealed by ultrafast microscopy. *ACS Photonics*, 5(1):105–110, 2018.
 - [9] A. Semenov, A. Nitzan. Electron transfer in confined electromagnetic fields. *J. Chem. Phys.*, 150(17):174122, 2019.
 - [10] K. Takazawa, J. Inoue, K. Mitsuishi, and T. Takamasu. Fraction of a millimeter propagation of exciton polaritons in photoexcited nanofibers of organic dye. *Phys. Rev. Letters*, 105:067401, 2010.
 - [11] D.M. Coles, P. Michetti, C. Clark, W.C. Tsoi, A.M. Adawi, J.-S. Kim, and D.G. Lidzey. Vibrationally assisted polariton-relaxation processes in strongly coupled organic-semiconductor microcavities. *Advanced Functional Materials*, 21(19):3691–3696, 2011.
 - [12] S. Baieva, O. Hakamaa, G. Groenhof, T. T. Heikkil, and J. J. Toppari. Dynamics of strongly coupled modes between surface plasmon polaritons and photoactive molecules: The effect of the stokes shift. *ACS Photonics*, 4(1):28–37, 2017.
 - [13] R. J. Holmes and S. R. Forrest. Strong exciton-photon coupling and exciton hybridization in a thermally evaporated polycrystalline film of an organic small molecule. *Phys. Rev. Lett.*, 93:186404, Oct 2004.
 - [14] L. Mazza, L. Fontanesi, and G. C. La Rocca. Organic-based microcavities with vibronic progressions: Photoluminescence. *Phys. Rev. B*, 80(23):235314, 2009.
 - [15] Y. Toyozawa. On the dynamical behavior of an exciton. *Progr. Theor. Phys. Suppl.*, 12:111–140, 1959.
 - [16] M. Reitz, C. Sommer, C. Genes. Langevin Approach to Quantum Optics with Molecules. *Phys. Rev. Lett.*, 122:203602, 2019.
 - [17] T.E. Li, J.E. Subotnik, A. Nitzan. Cavity molecular dynamics simulations of liquid water under vibrational ultrastrong coupling. *Proceedings of the National Academy of Sciences*, 117(31):18324–18331, 2020.
 - [18] L. Fontanesi, L. Mazza, and G. C. La Rocca. Organic-based microcavities with vibronic progressions: Linear spectroscopy. *Phys. Rev. B*, 80(23):235313, 2009.
 - [19] P. Michetti and G.C. La Rocca. Exciton-phonon scattering and photoexcitation dynamics in *j*-aggregate microcavities. *Phys. Rev. B*, 79:035325, Jan 2009.
 - [20] T. Skettrup. Microscopic approach to polaritons. *Phys. Rev. B*, 24:884–891, Jul 1981.
 - [21] F. Bassani A. Quattropani, L. C. Andreani. Quantum theory of polaritons with spatial dispersion: Exact solutions. *Il Nuovo Cimento D*, 7:55 – 69, 1986.
 - [22] H. Haug and S. W. Koch. *Quantum theory of the optical and electronic properties of semiconductors*. World Scientific, Singapore, 2001.
 - [23] N.J. Hestand and F.C. Spano. Expanded theory of h- and j-molecular aggregates: The effects of vibronic coupling and intermolecular charge transfer. *Chemical Reviews*, 118(15):7069–7163, 2018. PMID: 29664617.
 - [24] William H. Miller. On the relation between the semiclassical initial value representation and an exact quantum expansion in time-dependent coherent states. *The Journal of Physical Chemistry B*, 106(33):8132–8135, 2002.
 - [25] D.V. Shalashilin and M.S. Child. The phase space ccs approach to quantum and semiclassical molecular dynamics for high-dimensional systems. *Chemical Physics*, 304(1):103 – 120, 2004. Towards Multidimensional Quantum Reaction Dynamics.
 - [26] E. Artacho and D.D. O’Regan. Quantum mechanics in an evolving hilbert space. *Physical Review B*, 95:115155, 2017.
 - [27] M. Werther and F. Grossmann. Apoptosis of moving, non-orthogonal basis functions in many-particle quantum dynamics. 2019.
 - [28] B. D. Fainberg. *Opt. Spectrosc.*, 63:436, 1987. [Opt. Spektrosk., v. 63, 738 (1987)].
 - [29] B. D. Fainberg and D. Huppert. *J. Mol. Liquids*, 64:123, 1995. Erratum, v. 68, 281 (1996).
 - [30] Yu. T. Mazurenko and V. A. Smirnov. Stochastic description of the vibronic spectra of complex molecules. part 2. a model for an optically active brownian oscillator.
 - [31] S. Mukamel. *Principles of Nonlinear Optical Spectroscopy*. Oxford University Press, 1995.
 - [32] K. Takazawa, Y. Kitahama, Y. Kimura, and G. Kido. Optical waveguide self-assembled from organic dye molecules in solution. *Nano Letters*, 5(7):1293–1296, 2005.
 - [33] B.D. Fainberg. Mean-field electron-vibrational theory of collective effects in photonic organic materials. long-range frenkel exciton polaritons in nanofibers of organic dye. *AIP Advances*, 8(7):075314, 2018.
 - [34] B.D. Fainberg. Study of electron-vibrational interaction in molecular aggregates using mean-field theory: From exciton absorption and luminescence to exciton-polariton dispersion in nanofibers. *J. Phys. Chem. C*, 123(12):7366–7375, 2019.
 - [35] T. Brougham, G. Chadzitaskos, and I. Jex. Transformation design and nonlinear hamiltonians. *Journal of Modern Optics*, 56(14):1588–1597, 2009.
 - [36] The eigenvectors $|q, (u, M)\rangle$ have explicit representation in the basis of A_q and B_q operators (Ref.³⁵). The action of operators: $Q_q^\dagger |q, (u, M)\rangle = \sqrt{u+1} |q, (u+1, M+1)\rangle$; $Q_q |q, (u, M)\rangle = \sqrt{u} |q, (u-1, M-1)\rangle$; $P_q^\dagger |q, (u, M)\rangle = \sqrt{M-u+1} |q, (u, M+1)\rangle$; $P_q |q, (u, M)\rangle = \sqrt{M-u} |q, (u, M-1)\rangle$
 - [37] $c|\sigma\rangle = \sigma|\sigma\rangle$, $c^\dagger|\sigma\rangle = \sigma^*|\sigma\rangle$; completeness: $\mathbf{1} = \int \frac{d^2\sigma}{\pi} |\sigma\rangle\langle\sigma|$; the scalar product $\langle\sigma'|\sigma\rangle = e^{-\frac{|\sigma'-\sigma|^2}{2}}$